

# Color Portion of Solar Radiation in the Partial Annular Solar Eclipse, October 3<sup>rd</sup>, 2005, at Helwan, Egypt

A. H. Hassan, U. A. Rahoma, M. Sabry, A. M. Fathy

## Abstract

Measurements were made of various solar radiation components, global, direct and diffuse and their fractions during the partial annular solar eclipse on October 3<sup>rd</sup>, 2005 at Helwan, Egypt (Lat. 29.866° N and Long. 31.20° E), and an analysis has been made. The duration of the solar eclipse was 3 h 17 min, and the maximum magnitude of the eclipse in this region was 0.65. The optical depth of the direct component and the relative humidity decreased, while both the transparency and the air temperature increased towards the maximum eclipse. The general trends of the global components are decreasing optical depth and increasing transparency between the first contact and the last contact. The prevailing color during the eclipse duration was diffused infrared (77 % of the total diffuse radiation level).

**Keywords:** diffuse infrared solar radiation, partial solar eclipse, meteorological data, optical depth, transparency, linke turbidity and Angstrom turbidity.

## 1 Introduction

The greatest eclipse is defined as the instant when the axis of the Moon's shadow passes closest to the Earth's center. For total eclipses, the instant of greatest eclipse is virtually identical to the instants of greatest magnitude and greatest duration. However, for annular eclipses, the instant of greatest duration may occur either at the time of greatest eclipse or near the sunrise and sunset points of the eclipse path. On Monday October 3<sup>rd</sup>, 2005, a partial annular solar eclipse of the Sun was visible from within a narrow corridor which traversed half the Earth. The instant of greatest eclipse occurred at 10:32 UT, when the axis of the Moon's shadow passed closest to the center of the Earth. The maximum duration of totality was 4 min 32 s; the Sun's altitude was 71°, and the path width was 162 km. The maximum magnitude was 0.95 at Lat. 12°8'N and Long.E [1].

Extinction may be caused by a molecular absorption that is wavelength-dependent and follows the Rayleigh formula. The molecular absorption appears in the form of absorption bands projected on to the continuous background spectrum. In a clear sky, at lower atmospheric layers in the wavelength range 500–650 nm, extinction has three known components. It consists of molecular absorption following Rayleigh scattering; absorption at a discrete wavelength by water vapor; and weakening by the Chappuis band of ozone [2]. The absorbing components of the atmosphere are O<sub>2</sub>, O<sub>3</sub>, H<sub>2</sub>O, CO<sub>2</sub>, N<sub>2</sub>, O, N, NO, N<sub>2</sub>O, CO, CH<sub>4</sub> and their isotopic modifications, though the contributions of the latter are small. Spectra due to electronic transitions of molec-

ular and atomic of O, N, O<sub>3</sub>, lie chiefly in the ultraviolet region, while those due to the vibration and rotation of polyatomic molecules such as H<sub>2</sub>O, CO<sub>2</sub> and O<sub>3</sub>, lie in the infrared region. There is a very little absorption in the visible region. As the absorption coefficients associated with electronic transitions are generally very large, much of the UV is absorbed in the upper layers of the atmosphere. Some of the Oxygen and Nitrogen molecules are dissociated into atomic Oxygen and Nitrogen owing to absorption of the solar radiation, while other molecules are ionized. Dissociated atomic Oxygen and Nitrogen are also able to absorb solar radiation of still shorter wavelength, and some of these atoms become ionized as a result. The ionized layers in the upper atmosphere are formed mainly because of these processes. Owing to the very strong absorption by O<sub>2</sub>, N<sub>2</sub>, O, N and O<sub>3</sub> in the spectral region up to about 300 nm, the solar radiation in this region does not reach the earth's surface. In the visible region, there is some absorption due to the weak Chappuis bands of ozone and due to the red bands of molecular Oxygen which occur at about 690 and 760 nm. IR absorption by water vapor occurs at about 700, 800, 900, 1 100, 1 400, 1 900, 2 700, 3 200 and 6 300 nm and by CO<sub>2</sub> at about 1 600, 2 000, 2 700 and 4 300 nm. These bands play a part in the absorption in the lower atmosphere, below 50 km, where water vapor and CO<sub>2</sub> are largely concentrated. No photochemical action is associated with absorption in this region, and the absorbed energy is used entirely to heat the lower atmosphere [3].

Many studies of the variation of solar radiation and transparency have been carried out in recent years, dealing with solar eclipse totality and partial-

ity in different countries. A study of atmospheric responses due to the 11 August total solar eclipse in Romania, conducted by Copaciu and Yousef (1999), indicated that both global radiation and UVB radiation dropped dramatically to a minimum around totality. There was an opportunity to study the attenuation of such radiation due to clouds. The net radiation became negative for about 17 minutes at Căldărusani. The temperature dropped to about 30 °C soon after totality at both Afumati and Clarasi, although at the beginning of the eclipse it was about 46.5 °C at Afumati and 34 °C at Căalăarasi. At Căldărusani, the surface temperature dropped from 34.1 °C to 29 °C. It seems likely that the air temperature inside the umbra is between 29–30 °C. The response time of minimum surface temperature was about 18 minutes, which is comparable to the duration of the negative part of the net radiation when the backward radiation became higher than the incident radiation [4]. Studies of simultaneous measurements of radiation; photolysis frequencies, O<sub>3</sub>, CO, OH, PAN and NO<sub>x</sub> species were carried out in the boundary layer, along with the relevant meteorological parameters, under total solar eclipse conditions [5]. This experiment, performed at about 34 solar zenith angles and under noontime conditions, thus provided a case study of the interactions between radiation and photochemistry under fast “day-night” and “night-day” transitions, at high solar elevation. The results revealed a close correlation between photolysis frequencies and the UV radiation flux. Due to the decreasing fraction of direct radiation at shorter wavelengths, all three parameters showed much weaker cloud shading effects than global solar radiation. NO and OH concentrations decreased to essentially zero during totality. Subsequently, NO and OH concentrations increased almost symmetrically with their decrease preceding totality. The NO/NO<sub>2</sub> ratio was proportional to NO<sub>2</sub> over ±30 min before and after totality, indicating that the partitioning of NO<sub>x</sub> species was determined by JNO<sub>2</sub>. Simple box model simulations show the effect of reduced solar radiation on the photochemical production of O<sub>3</sub> and PAN. A study was made of the depression of the different solar radiation components during the solar eclipse, August 11<sup>th</sup>, 1999, over Egypt (as a partial solar eclipse, 70 % covering of the solar disk in Helwan, Egypt) [6]. The maximum depression values in the different components of solar radiation was 54 % in red solar radiation (for global and direct), while the minimum depression was in infrared solar radiation (34 % for global and 41 % for direct). The clearness index and the diffuse fraction were 0.634 and 0.232, respectively. The atmospheric red radiation was 7.4 % and the atmospheric infrared radiation was 10.7 %. The percentage of ultraviolet was 3 %. A study of the spectral composition of

global solar radiation by interference metallic filters was carried out during the same previous eclipse in August 11<sup>th</sup>, 1999 in Helwan, Egypt [7]. The conclusions indicated an increase in the whole interval from 350–450 nm but without risk to the human eye. This interval lies at the end of ultraviolet solar radiation, while the minimum variation lies between 500–700 nm. This interval represents the normal maximum peak of the solar spectrum, and goes up to the 700–900 nm band. The change in the meteorological parameters is related to the variability of the solar spectrum shift from the short wave band to the long wave band. The maximum drop in the solar spectrum lies in the interval that consists of the normal peak of the solar spectrum from 500–600 nm. An investigation was made of the effects of pollutants on the color portion, where the increase in pollutants reduces the violet-blue band by 11 %, the green-yellow band by 14 %, the red band by 13 % and the infrared band by 5 % of the average annual values [8].

Using ground-based spectral radiometric measurements taken over the Athens atmosphere in May 1995, an investigation was carried out of the influence of gaseous pollutants and aerosols on the spectral radiant energy distribution. It was found that the spectral measurements exhibited variations based on various polluted urban atmospheric conditions, as determined by gaseous pollutants record analysis. The relative attenuations caused by gaseous pollutants and aerosols can exceed 27 %, 17 % and 16 % in the global ultraviolet, visible and near infrared portions of the solar spectrum, respectively, as compared to “background” values. In contrast, an enhancement of the near infrared diffuse component by 66 % was observed, while in the visible and ultraviolet bands the relative increases were 54 % and 21 %, respectively [9].

The aim of the present work is to study and determine the percentage of color portion variations for the different solar radiation components during the solar eclipse on October 3<sup>rd</sup>, 2005 at Helwan, Egypt.

## Instruments and Measurements

Equipment was installed on the roof of the National Research Institute of Astronomy and Geophysics (NRIAG) building in Helwan, (29°54'N 30°20'E, 126 m elevation above sea level). The background is taken as desert and pollution. Measurements were conducted from sunrise to sunset. The time of measurements was taken as the local mean time of Cairo (GMT+2 hours).

The instruments used in this work were:

- A pyrliometer for measuring the direct solar radiation, in three different bands, direct yellow (Y) (530–2800 nm), direct red (R) (630–2800 nm), direct

infrared (IR) (695–2800 nm), and also the total direct band (I) (280–2800 nm).

- Four pyranometers for measuring the different components of global solar radiation ( $G$ , 280–2800 nm), global ultraviolet ( $G_{UV}$ , 285–385 nm), global infrared ( $G_{IR}$ , 695–2800 nm) and a black-and-white type sensor to measure the diffuse ( $D$ , 280–2800 nm) solar radiation.
- A meteorological station to measure the different meteorological parameters.

## Theoretical background

To calculate the extraterrestrial solar radiation at any time during the partial solar eclipse, we carried out the following:

$$E_i \text{ at eclipse} = (E_i)(1 - M) \quad (1)$$

where  $E_i$  is substituted by any radiation quantity, e.g.  $G_o$ ,  $G_{IR_o}$ ,  $G_{UV_o}$ ,  $B_1$ ,  $B_2$ ,  $B_3$  and  $B_4$ . Optical depth ( $\alpha$ ) and transparency ( $\tau$ ) are calculated by the formula:

$$I_{b\lambda} = I_{o\lambda} \exp(-\alpha m) \quad (2)$$

where  $\alpha$  and  $\tau$  may be calculated as

$$\alpha = -\ln(I_{b\lambda}/I_{o\lambda})(1/m) \quad (3)$$

$$\tau = 1/\exp(\alpha \cdot m). \quad (4)$$

The calculations of the extraterrestrial solar radiation for the bands of various components bands are based on [10].

The diffuse infrared ( $D_{IR}$ ) was calculated from the equation:

$$D_{IR} = G_{IR} - IRCOS(\Theta) \quad (5)$$

The Linke turbidity factor,  $LT$  is given by:

$$LT = \frac{1}{\delta_R m_A} \cdot \ln \cdot \left[ \frac{I_0}{I} \right] \quad (6)$$

where  $\delta_R$  is given by:

$$\delta_R = \frac{1}{9.4 + 0.9 \cdot m_A} \quad (7)$$

where  $m_A$  is given by:

$$m_A = \left[ \frac{P}{1013.25} \cdot \frac{1}{\cos \theta + 0.15(93.885 - \theta)^{-1.253}} \right] \quad (8)$$

The total amount of water vapor in the atmosphere in the vertical direction is highly variable and depends on the instantaneous local conditions. This amount, expressed as precipitable water  $W$  (cm), and can be readily computed through a number of standard routine atmospheric observations. The precipitable water vapor can vary from 0.0 to 5 cm [11, 12].

$$W = \left[ \frac{0.493 \cdot (\Phi_r) \cdot \exp[26.23 - (5416/t_k)]}{T_k} \right] \quad (9)$$

The Angstrom turbidity coefficient is a dimensionless index that represents the amount of aerosol, and the relation between the Linke turbidity ( $LT$ ) and the Angstrom turbidity ( $\beta$ ) for Helwan is [13]:

$$\beta = -0.194933 + 0.0620059LT \quad (10)$$

## Results and discussion

Table 1 characterizes the phase and magnitude (the fraction of the sun’s diameter covered at mid eclipse) at different stages of the partial solar eclipse under study at Helwan, Egypt. The duration of the solar eclipse was 3 h 05 m, with maximum magnitude in this region of 0.65 [1].

Table 1: Characterization of the partial solar eclipse, 3–10–2005 at Helwan

Eclipse Phase	Magnitude	hh:mm:ss	$a$	$Az$
<i>S.P.E</i>	0	10:27:14.4	51	149
<i>M.E</i>	0.65	11:59:11.2	56	187
<i>E.P.E</i>	0	13:31:41.3	47	222

Table 2 characterizes the environmental and meteorological conditions of the eclipse day in Helwan, e.g. sunrise ( $S.R$ ), upper transit of the sun ( $T.S$ ), sunset ( $S.S$ ), dry-bulb temperature ( $T_d$ ), wet-bulb temperature ( $T_w$ ), air pressure ( $P$ ), cloud cover ( $Cl.$ ), visibility ( $Vis.$ ), relative humidity ( $R.H$ ) and dew point ( $D.P$ ).

Fig. 1 shows the temporal measurements of the hourly variation of various global solar radiation components, global horizontal ( $G$ ), global infrared horizontal ( $G_{IR}$ ) and total diffuse horizontal ( $D$ ) as well as the extraterrestrial solar radiation,  $G_o$  in ( $W/m^2$ ).

Table 2: Characterization and environmental conditions of the eclipse day

<i>S.R</i> hh:mm	<i>T.S</i> hh:mm	<i>S.S</i> hh:mm	$T_d$ °C	$T_w$ °C	$P$ hPa	$Cl.$ Okta	$Vis.$ Km	$R.H$ %	$D.P$ °C
05:48	11:43	17:38	29.1	21.88	999.62	0	5.0	54.6	18.62

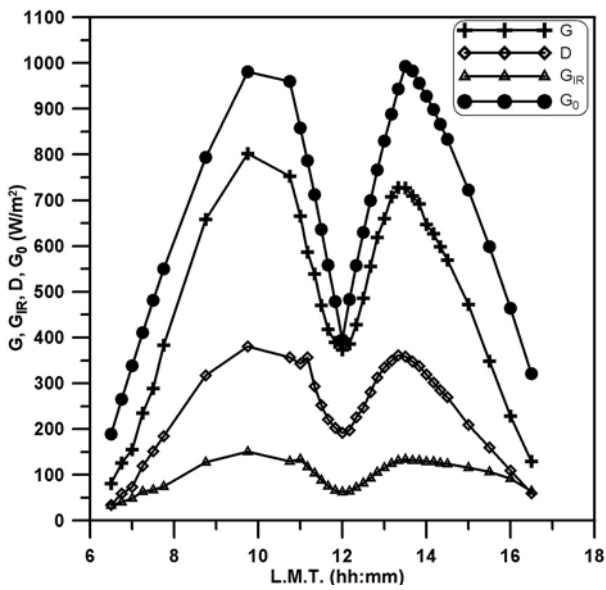


Fig. 1: Hourly variation of  $G$ ,  $G_{IR}$ ,  $D$  and  $G_0$

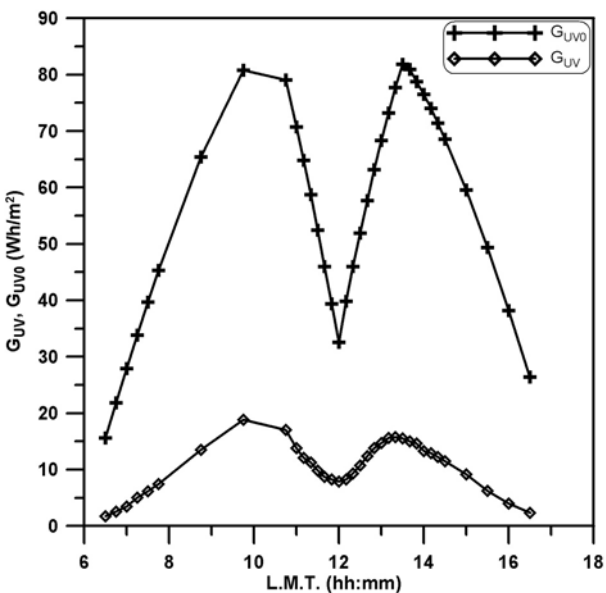


Fig. 2: Hourly variation of  $G_{UV}$ , and  $G_{UV0}$

This figure clearly shows the depression of the irradiance of all components due to the eclipse, while the depression of the diffuse radiation is lower, because of the percentage of direct change to diffuse through the layer of atmosphere. Fig. 2 shows the hourly variation measurements of global ultraviolet solar radiation ( $G_{UV}$ ) along with the extraterrestrial global ultraviolet solar radiation ( $G_{UV0}$ ). Fig. 3 shows the hourly variation measurements of various direct solar radiation components: total direct (I), direct yellow (Y), direct red (R) and direct infrared (IR), in ( $W/m^2$ ). The depression gradient starting from the total to infrared bands passing through the yellow and red bands before and after the eclipse is clearly shown in the graph, but the

difference between the bands is narrow during the maximum eclipse.

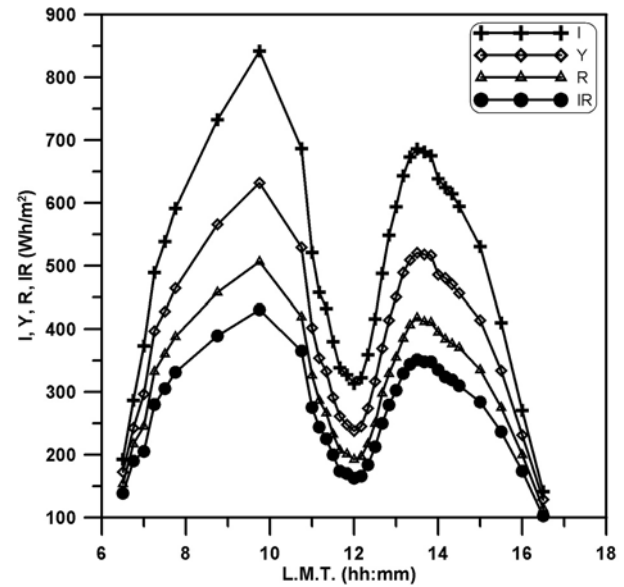


Fig. 3: Hourly variation of  $I$ ,  $Y$ ,  $R$  and  $IR$

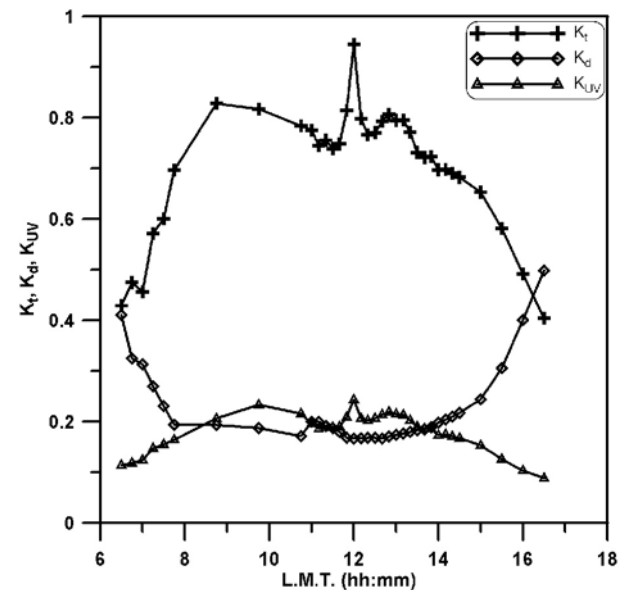


Fig. 4: Hourly variation of  $K_t$ ,  $K_d$  and  $G_{UV}$

Fig. 4 shows the hourly variation of various clearness indices, e.g.  $K_t$ ,  $K_{UV}$  and diffuse fraction  $K_d$ . The clearness indices have higher values during the eclipse, while the  $K_d$  value suffers no variation because the percentage decrease of diffuse is equal to the percentage decrease of the global value. Fig. 5 shows information on the meteorological conditions before, during and after the partial solar eclipse at Helwan site, i.e. dry-bulb temperature ( $T_d$ ) and relative humidity (RH %). The decrease in ambient temperature and the increase in relative humidity are

recorded as 1.8 °C and 2 %, respectively, as the difference between the first contact and the maximum eclipse. Fig. 6 shows the hourly variation of the color portion of the direct bands  $B_1$ ,  $B_2$ ,  $B_3$  and  $B_4$  over the whole day from sunrise to sunset. The highest short wavelength values ( $B_1$  and  $B_2$ ) over the day are at low air mass (around true noon), while the top long wavelength value ( $B_4$ ) is at higher air mass near sunrise and sunset.

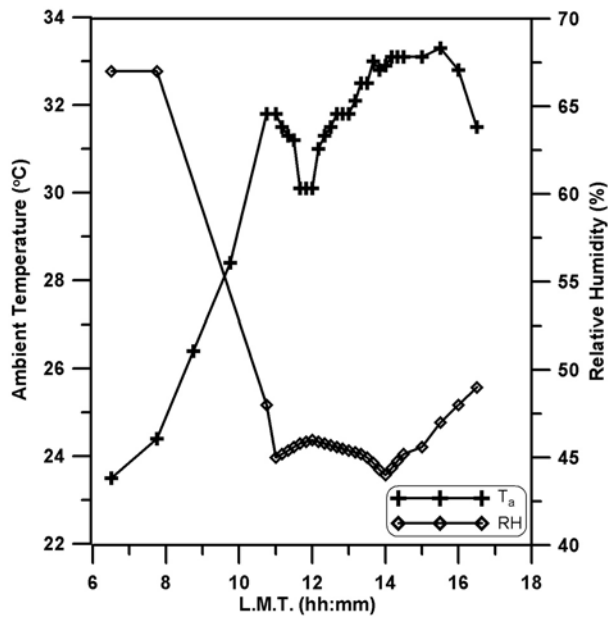


Fig. 5: Hourly variation of ambient temperature and relative humidity

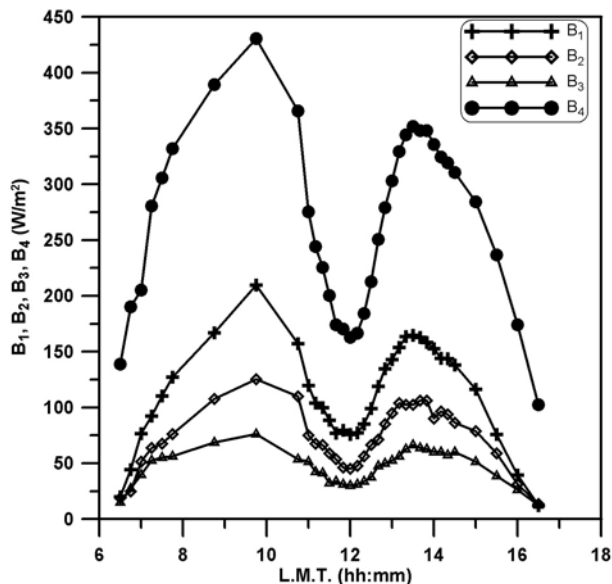


Fig. 6: Hourly variation of  $B_1$ ,  $B_2$ ,  $B_3$  and  $B_4$

Fig. 7 shows the hourly variation of the horizontal global infrared  $G_{IR}$  and the direct infrared IR over the whole day. The IR component is predominant outside the eclipse period, but this changes during

an eclipse. The difference between  $G_{IR}$  and IR is the diffuse infrared ( $D_{IR}$ ) that appears in Equation 5. It is clear from this figure that the direct infrared is dominant before and after the eclipse, but during the eclipse, the global infrared is dominant. Fig. 8 shows the hourly variation of the irradiance of the total diffuse  $D$  and the diffuse infrared  $D_{IR}$ , where it is clear that the total diffuse radiation values were higher than the diffuse infrared radiation values before, after and during the eclipse. Fig. 9 shows the ratio (RD) of diffuse infrared ( $D_{IR}$ ) to the total diffuse, where the maximum ratio RD conjugates with the maximum eclipse, and the duration of RD conjugates with the duration of the eclipse.

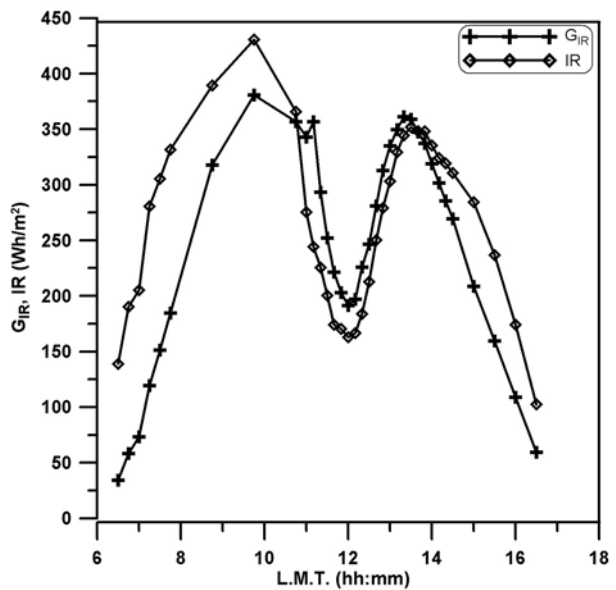


Fig. 7: Hourly variation of IR and  $G_{IR}$

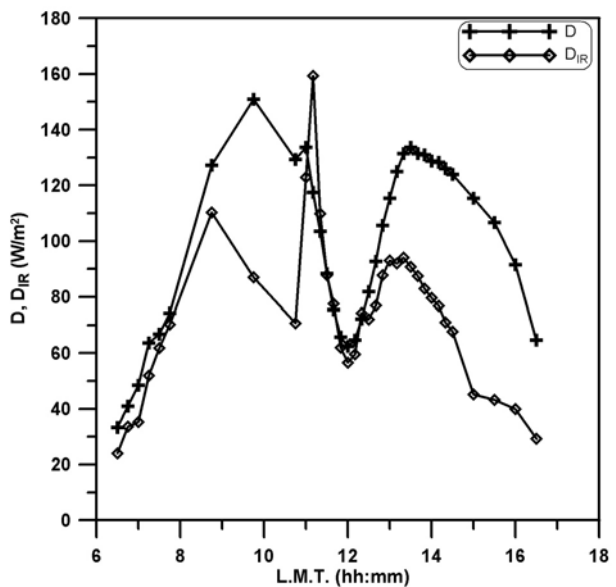


Fig. 8: Hourly variation of  $D$  and  $D_{IR}$

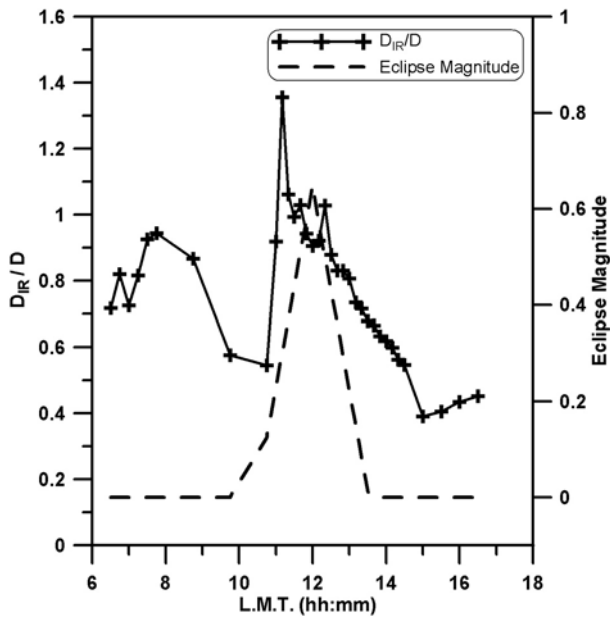


Fig. 9: Hourly variation of  $D_{IR}/D$  along with the Eclipse magnitude

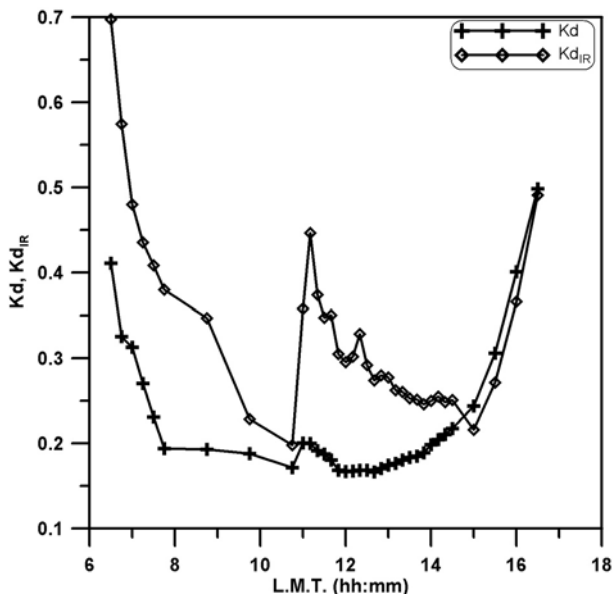


Fig. 10: Hourly variation of  $Kd$  and  $Kd_{IR}$

Fig. 10 compares the total diffuse fraction  $Kd$  with the infrared diffuse fraction  $Kd_{IR}$ . The top value of  $Kd_{IR}$  was very near sunrise and sunset (high air mass) and near the maximum of the eclipse, while the top  $Kd$  value was very near sunrise and sunset only, while the minimum value was in the middle of the day (low air mass). Fig. 11 shows the different percentage of the color portion ( $C-P$ ) through the day from 0800 to 1600, passing through the different intervals of the eclipse for the different bands. This figure shows that the prevailing color in the clear case is  $IB_4 > IB_1 > IB_2 > IB_3$ . These results agree with

Figs. 7 and 9, where the prevalent color during the eclipse is diffuse infrared. The percentage of the color portion at the true eclipse interval shows the same trend. However, the  $C-P$  in the direct infrared  $IB_4$  during the eclipse is low, while the high values are very near to sunrise and sunset, where there are high air masses, which are the major causation of the absorption and scattering of the infrared wavelengths. Generally, the results for the color portion agree with previous work in this location [8].

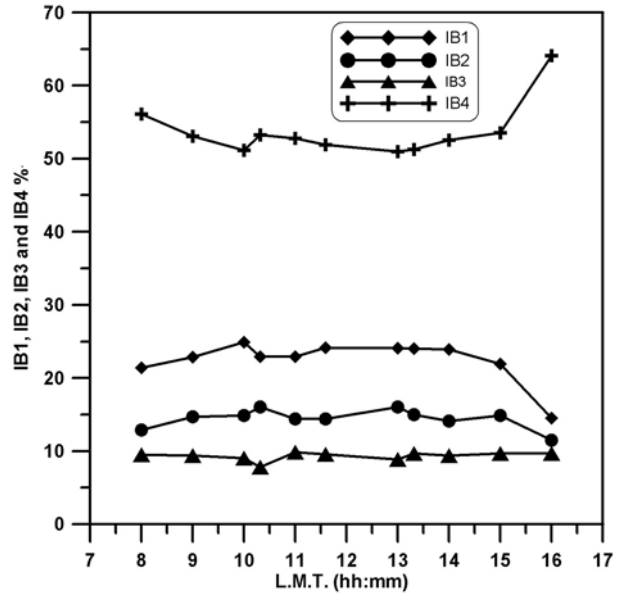


Fig. 11: Variation of color portion of the different bands over the day of eclipse

Table 3 presents the hourly variation of the optical depth ( $\alpha$ ) and transparency ( $\tau$ ) from 0800 to 1600 through the duration of the eclipse of the global ( $G$ ), global infrared ( $G_{IR}$ ), global ultraviolet ( $G_{UV}$ ), total direct ( $I$ ) as well as direct color bands  $IB_1$ ,  $IB_2$ ,  $IB_3$  and  $IB_4$ . This table demonstrates that the top optical depth ( $\alpha$ ) and low transparency ( $\tau$ ) are for the  $G_{UV}$ , where the low transparency for  $G_{UV}$  has two causes. Firstly, the intensity of the scattered light is proportional to  $1/\lambda^4$  and to the square of the volume of the particle [10, 11]. This means that the intensity of the scattering of UV light is eleven times the scattering of red light. This region is characterized by the high pollutant limit and the large size of the pollutants (mainly Ca and Fe) [8, 14]. Secondly, the ozonosphere absorbs a large amount of this band.

Generally, the transparency increases gradually from the short wavelength to the long wavelength. The general trend of the global components in  $G$  and  $G_{IR}$  is the low optical depth ( $\alpha$ ) and high transparency ( $\tau$ ). The coefficient of the atmospheric attenuation is directly proportional to the wavelength, showing a general reddening. At maximum eclipse, the optical depth ( $\alpha$ ) is less and the transparency ( $\tau$ )

is higher in all bands. This is because the air temperature decreased by 1.8 °C and the R.H increased by 2 %, as shown in Fig. 5, due to the low thickness of the atmospheric layers and, accordingly, lower optical thickness and higher transparency where the relation between transparency and temperature is inverted [7].

Table 4 presents the different values of Linke turbidity (LT), Angstrom turbidity ( $\beta$ ), precipitable water ( $W$ , cm), total diffuse fraction  $Kd$  and infrared diffuse fraction  $Kd_{IR}$  during the day passing through the eclipse period.

Both Linke and Angstrom turbidity values are higher in the afternoon than in the morning. This is because of the high temperature in the afternoon, which expands and excites the gases and the dust in the atmosphere. The distribution of precipitable water ( $W$ ), diffuse fraction  $Kd$  and the diffuse infrared fraction  $Kd_{IR}$  give the concept of the atmospheric character through the eclipse. The high values of LT and  $\beta$  and  $W$  give an idea of the high turbidity of the day of observation. The prevailing color throughout the duration of the eclipse was diffuse infrared (77 % of the total diffuse).

Table 3: Various optical depth values ( $\alpha$ ) and transparency values ( $\tau$ ) during the day, including the phases of the eclipse (from the FC to the ME to LC) of  $G$ ,  $G_{IR}$ ,  $G_{uv}$ ,  $I$ ,  $B_1$ ,  $B_2$ ,  $B_3$  and  $B_4$

		8:00	9:00	10:00	10:31 F.C	11:00	11:59 M.E	13:00	13:31 L.C	14:00	15:00	16:00
G	$\tau$	0.696	0.829	0.818	0.784	0.796	0.945	0.796	0.732	0.697	0.653	0.492
	$\alpha$	0.125	0.100	0.136	0.190	0.202	0.047	0.182	0.237	0.257	0.245	0.282
$G_{IR}$	$\tau$	0.657	0.783	0.759	0.727	0.781	0.798	0.789	0.707	0.672	0.565	0.459
	$\alpha$	0.148	0.132	0.191	0.254	0.201	0.190	0.192	0.269	0.288	0.334	0.315
$G_{UV}$	$\tau$	0.164	0.207	0.233	0.216	0.196	0.243	0.215	0.190	0.173	0.154	0.104
	$\alpha$	0.622	0.838	0.991	1.200	1.300	1.172	1.226	1.265	1.249	1.078	0.901
I	$\tau$	0.432	0.535	0.615	0.574	0.494	0.654	0.558	0.508	0.466	0.388	0.198
	$\alpha$	0.289	0.333	0.331	0.434	0.563	0.352	0.465	0.516	0.544	0.674	0.645
B1	$\tau$	0.360	0.473	0.594	0.509	0.449	0.613	0.521	0.474	0.433	0.329	0.112
	$\alpha$	0.352	0.398	0.354	0.528	0.639	0.405	0.520	0.568	0.596	0.641	0.870
B2	$\tau$	0.422	0.595	0.692	0.696	0.539	0.712	0.676	0.575	0.498	0.436	0.173
	$\alpha$	0.297	0.276	0.250	0.285	0.493	0.281	0.312	0.421	0.476	0.478	0.698
B3	$\tau$	0.563	0.689	0.764	0.615	0.664	0.585	0.476	0.673	0.601	0.531	0.263
	$\alpha$	0.198	0.198	0.183	0.383	0.327	0.444	0.592	0.301	0.362	0.365	0.532
B4	$\tau$	0.451	0.530	0.586	0.569	0.486	0.632	0.530	0.485	0.456	0.387	0.237
	$\alpha$	0.274	0.338	0.363	0.444	0.576	0.380	0.506	0.551	0.559	0.547	0.573

Table 4: The different values of Linke turbidity (LT), Angstrom turbidity ( $\beta$ ), precipitable water ( $W$ ), total diffuse fraction  $Kd$  and infrared diffuse fraction  $Kd_{IR}$  during the day passing through the eclipse period

	8:00	9:00	10:00	10:31 F.C	11:00	11:59 M.E	13:00	13:31 L.C	14:00	15:00	16:00
LT	3.541	3.754	3.608	4.657	3.608	3.749	3.749	5.578	5.888	6.071	7.630
$\beta$	0.024	0.038	0.028	0.094	0.028	0.037	0.037	0.151	0.170	0.181	0.278
W	3.296	3.128	2.922	3.402	3.440	3.365	3.470	3.575	3.918	3.756	3.710
Kd	0.194	0.193	0.188	0.172	0.192	0.167	0.175	0.184	0.199	0.244	0.401
$Kd_{IR}$	0.380	0.347	0.228	0.198	0.358	0.295	0.278	0.253	0.250	0.216	0.366

## 2 Conclusion

The results obtained from this analysis of the spectral composition of global and direct irradiance show that various atmospheric parameters cause considerable changes to the spectral distribution of radiant energy reaching the ground. Our conclusions are summarized as follows:

1 – The percentage of prevalent color during the day is  $B_4 > B_1 > B_2 > B_3$ . The predominant colors during the eclipse were infrared, blue, green and yellow, respectively. The variation of the color portion is clearly obvious in  $B_2$  and  $B_3$ , where the percentage was higher in  $B_2$  and lower in  $B_3$  during the eclipse period. The  $C-P$  of  $B_1$  and  $B_4$  underwent almost no change. The lowest percent of color portion was in the red.

2 – At maximum eclipse (ME), optical depth ( $\alpha$ ) is lower and transparency ( $\tau$ ) is higher. The air temperature decreased by  $1.8^\circ\text{C}$  and a 2 % increase in RH was recorded; this was due to the low thickness of the atmospheric layers. The optical thickness was therefore lower and, accordingly, this raised the transparency values. The general trend of the global components in  $G$ ,  $G_{IR}$  and  $G_{UV}$  are low optical depth ( $\alpha$ ) and high transparency ( $\tau$ ) in the first contact in comparison with the last contact. There was high optical depth ( $\alpha$ ) and low transparency ( $\tau$ ) in  $G_{UV}$ , where the ozonosphere and the air pollutants absorbed a large amount of this band. The top percentage of short wave length ( $IB_1$  and  $IB_2$ ) over the day was at low air mass (around true noon), while the top percentage of the long wavelength ( $IB_4$ ) was at higher air mass.

The prevalent color throughout the eclipse was diffuse infrared (77 % of the total diffuse).

## References

- [1] Espenak, F., Anderson, J.: Total Solar Eclipse of 2006 March 29. NASA/TP, 212762.
- [2] Green, Robin M.: *Spherical astronomy*. Cambridge University Press, 1993.
- [3] Robinson, N.: *Solar radiation*, Elsevier, London, 1966.
- [4] Copaciu, V., Yousef, S. M.: Some atmospheric responses the 11 August 1999 total solar eclipse near Bucharest. *Rom. Astron. J.* **9**, 1999, p. 19–23.
- [5] Fabian, P., Rappenglück, B., Stohl, A., Werner, H., Winterhalter, M., Schlager, H., Berresheim, H., Stock, P., Kaminski, U., Koepke, P., Reuder, J., Birmili, W.: Boundary layer photochemistry during a total solar eclipse. *Meteorologische Zeitschrift*, 2001, **10(3)**, 187–192.
- [6] Hassan, A. H., Shaltout, M. A. Rahoma, U. A.: The depression of different solar radiation components during the solar eclipse, 11 August 1999 over Egypt. *J. Astron. Soc. of Egypt*, 2004, **12(1)**, 70–81.
- [7] Rahoma, U. A., Shaltout, M. A., Hassan, A. H.: Study of spectral global solar radiation during the partial solar eclipse of 11 August, 1999 at Helwan, *Egypt. J. Astron. Soc. of Egypt*, 2004, **12(1)**, 31–45.
- [8] Shaltout, M. A., Ghoniem, M. M., Hassan, A. H.: Measurements of the air pollution effects on the color portions of solar radiation at Helwan, Egypt. *4th World Ren Energy Cong, USA*, 1996, **2**, 1 279–1 282.
- [9] Constantnose, P., Jacovides, Michael, D., Steven, Demosthenis, N., Asimakopoulos: Spectral solar irradiance and some optical properties for various polluted atmospheres. *Sol. Energy.* **69(3)**, 2000, p. 215–227.
- [10] Iqbal, M.: *An introduction to solar radiation*, Academic Press, 1983.
- [11] Kasten, F.: A simple parameterization of the pyr heliometric formula for determining the Linke turbidity factor. *Meteor. Rdsch.*, 1980, **33**, 124–127.
- [12] Louche, A., Peri, G., Iqbal, M.: An analysis of Linke turbidity factor. *Sol. Energy.*, **37(6)**, 124–127.
- [13] Hamdy, K. Elminir, Rahoma, U. A., Benda, V.: Comparison Between Atmospheric Turbidity Coefficients of Desert and Temperate Climates. *Acta Polytechnica*, 2001, **41(2)**.
- [14] Hala, S. Own, Hamdy, K. Elminir., Yasser, A. Abdel-Hady, Fathy, A. M.: Adaptation of wavelet features to predict the local noon erythema ultraviolet irradiance, *International Journal of Computational Intelligence Research (IJ-CIR)*, 2008, Issue 4 of Volume 4.

A. H. Hassan, U. A. Rahoma,  
M. Sabry, A. M. Fathy  
Phone: +20 227 044 422  
E-mail: mohamed.ma.sabry@gmail.com  
National Research Institute of Astronomy  
and Geophysics  
Helwan, Egypt

## Nomenclature

$a$	Altitude of the sun above the horizon
$Az$	Azimuth of the sun
$D.P.$	Dew point (Co)
$D$	Measured horizontal diffuse solar radiation
$D_{IR}$	Infrared diffuse solar radiation
$F.C$	First contact of eclipse
$G$	Global solar radiation, 280–2800 nm
$G_{IR}$	Horizontal infrared global solar radiation, 695–2800 nm
$G_o$	Extraterrestrial global solar radiation, 250–2800 nm
$G_{UV}$	Horizontal UV global solar radiation, 280–385 nm
$G_{UVo}$	Extraterrestrial UV global solar radiation, 250–385 nm
$I$	Direct solar radiation, 280–2800 nm
$B_1$	Value of band $I - Y = 280-530$ nm
$B_2$	Value of band $Y - R = 530-630$ nm
$B_3$	Value of band, 630–695 nm
$B_4$	Value of band, 695–2800 nm
$IB_1$	Color portion of $B_1$ as a percentage
$IB_2$	Color portion of $B_2$ as a percentage
$IB_3$	Color portion of $B_3$ as a percentage
$IB_4$	Color portion of $B_4$ as a percentage
$I_{b\lambda}$	Measured spectral irradiance at wavelength $\lambda$
$I_{o\lambda}$	Extraterrestrial spectral irradiance corrected for the actual sun – earth distance
$IR$	Direct infrared solar radiation, 695–2800 nm
$Kd$	Diffuse fraction (D/G)
$Kd_{IR}$	IR Diffuse fraction (diffuse infrared/global infrared = $D_{IR}/G_{IR}$ )
$Kt$	Clearness index ( $G/G_o$ )
$K_{UV}$	Clearness index of UV ( $G_{UV}/G_{UVo}$ )
$L.C$	Last contact of eclipse
$LT$	Linke turbidity factor
$M.E$	Maximum eclipse or mid eclipse
$m$	Air mass, $m = \sec\Theta$
$M$	Magnitude of the solar eclipse, defined as the fraction of the solar diameter that is obscured
$m_A$	Relative optical air mass
$P$	Air pressure (hPa)
$R.H$	Relative humidity (R.H)
$R$	Direct red solar radiation, 630–2800 nm
$RD$	Ratio of diffuse infrared to the total diffuse = $DIR/D$
$SPE$	Start of partial eclipse in local time (First contact)
$SR$	Sunrise
$SS$	Sunset
$S$	Measurements of sunshine duration (hour)
$S_o$	Calculation of sunshine duration (hour)
$T.S$	Upper transit of the sun
$T_d$	Dry-bulb temperature (°C)
$T_w$	Wet-bulb temperature (°C)
$T_k$	Ambient temperature in kelvins
$Y$	Direct yellow solar radiation, 530–2800 nm
$\alpha$	Optical depth for any bands
$\beta$	Angstrom turbidity coefficient
$\Theta$	Zenith angle
$\tau$	Transparency for any bands
$\delta_R$	Spectrally integrated optical depth of the clean dry atmosphere
$\Phi_r$	Relative humidity in fraction of one ( $\Phi_r = R \cdot H/100$ )